Wireless Crack Sensing Systems for Bridges

PREPARED BY:

Chenglin Wu, PhD

Missouri University of Science and Technology

PREPARED FOR:

Missouri Department of Transportation

Construction and Materials Division, Research Section

TECHNICAL REPORT DOCUMENTATION PAGE

| 1.   Report No.
cmr21-004	2. Government Accession No.	3. Recipient's Catalog No.
4. Title and Subtitle
Wireless Crack Sensing Systems for Bridges		**5. Report Date**
May 2021
Published: June 2021 |
| | | **6. Performing Organization Code** |
| **7. Author(s)**
   Chenglin Wu, PhD, https://orcid.org/0000-0001-7733-1084 | | **8. Performing Organization Report No.** |
| **9. Performing Organization Name and Address**
Missouri University of Science and Technology
132 Butler-Carlton Hall
1401 N. Pine St.
Rolla, MO 65409-0030 | | **10. Work Unit No.** |
| | | **11. Contract or Grant No.**
MoDOT project # TR202008 |
| **12. Sponsoring Agency Name and Address**
Missouri Department of Transportation (SPR-B)
Construction and Materials Division
P.O. Box 270
Jefferson City, MO 65102 | | **13. Type of Report and Period Covered**
Final Report (September 1, 2019-May 1, 2021) |
| | | **14. Sponsoring Agency Code** |

15. Supplementary Notes

16. Abstract
The main objective of this research was to develop and deploy a wireless crack sensing system that can measure and monitor cracks for both concrete and steel bridge structures. This system contained the sensing unit, wireless data transmitting system, as well as a data processing unit. The sensing unit consisted of single or arrays of advanced thin film-based sensing nodes that are capable to measuring crack induced strains in bridge structures. This thin film sensing node contained soft polymer film (polyvinylidene difluoride, PVDF) embedded with conductive nanoparticles (graphene) or atomically thin films. An additional fiber-coated sensor was explored as a sensor to detect large crack growth. The piezoresistive mechanism was considered to convert the strain to electrical resistance of the sensing unit. The sensing unit was also connected to a wireless transmitting system to broadcast the signal wirelessly. The wireless transmitting system utilized a blue-tooth technology that can enable the sensing unit to broadcast electronic signals in terms of electrical resistance. These signals were received by a mobile device (laptop or cellphone) that can convert the electrical resistance information into the measured stains. These measurements were processed using the data processing unit. The data processing unit received the electrical resistance data and converted it into measured strains. The machine learning approach was also taken to train the software to be able to automatically detect the abnormalities in the measured strain for critical crack growth detection.

| **17. Key Words**
Bridge; Cracking; Sensor; Nanocomposite; Graphene: Raspberry Pi, Cloud, Machine learning | **18. Distribution Statement**
No restrictions. This document is available through the National Technical Information Service, Springfield, VA 22161. | | |
|---|---|---|---|
| **19. Security Classif. (of this report)**
Unclassified. | **20. Security Classif. (of this page)**
Unclassified. | **21. No. of Pages**

51 | **22. Price** |

Wireless Crack Sensing Systems for Bridges

Project Number: TR202008

Final Report

Investigator

Dr. Chenglin Bob Wu, Assistant Professor

Missouri S&T

May 2021

COPYRIGHT

DISCLAIMER

ACKNOWLEDGMENTS

EXECUTIVE SUMMARY

The main objective of this research was to develop and deploy a wireless crack sensing system that can measure and monitor cracks for both concrete and steel bridge structures. This system contains the sensing unit, wireless data transmitting system, as well as a data processing unit. The sensing unit consists of single or arrays of advanced thin film-based sensing nodes that are capable of measuring crack induced strains in bridge structures. This thin film sensing node contains soft polymer film (polyvinylidene difluoride, PVDF) embedded with conductive nanoparticles (graphene) or atomically thin films. Both the Poisson's effect and contact mechanism were considered to covert the strain to electrical resistance of the sensing unit. This sensing unit is also connected to a wireless transmitting system to broadcast the signal wirelessly. The wireless transmitting system utilizes a blue-tooth technology that can enable the sensing unit to broadcast electronic signals in terms of electrical resistance. These signals were received by a mobile device (laptop or cellphone) that can convert the electrical resistance information into the measured stains. These measurements are processed using the data processing unit. The data processing unit receives the electrical resistance data and converts it into measured strains. The machine learning approach was also taken to train the software to be able to automatically detect the abnormalities in the measured strain for critical crack growth detection.

Keywords: Bridge; Cracking; Sensor; Nanocomposite; Graphene: Raspberry Pi, Cloud, Machine learning

CONTENTS

LIST OF FIGURES

1. INTRODUCTION

1.1 Problem Statement

1.1.1 Corrosion and cracking

Corrosion is one of most critical reliability issues of our crumbling civil infrastructure as shown in Fig. 1a-c. The annual budget for repairs and maintenances caused by corrosion is about $1 trillion considering inflation in 2013, $276 billion at 1998, and actual cost paid at least $552 billion [1] as illustrated in Fig. 1d. In addition, the corrosion induced structural cracking and failures are most common for bridge structures constructed either with structural steel or reinforced concrete, which can cause catastrophic failures that may lead to loss of human lives. Therefore, monitoring corrosion induced strain and failures and providing timely warning are essential to the daily operations of transportation infrastructure.
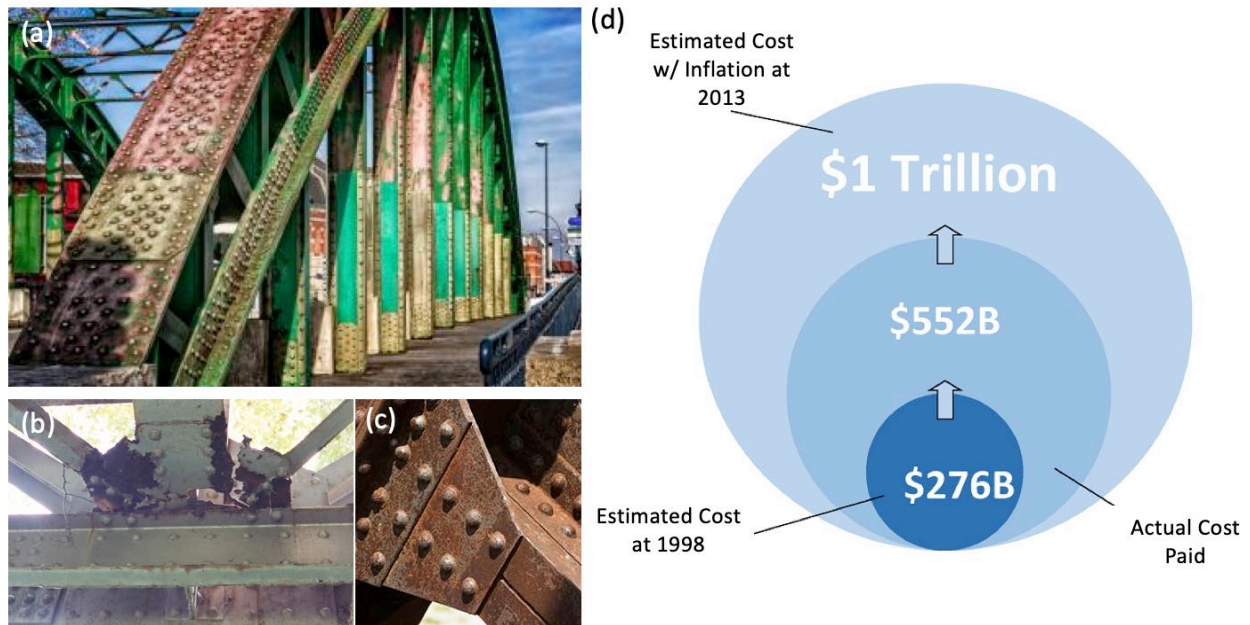
Fig. 1: (a)-(c) Corrosion induced structural failures for steel bridges; (d) associated cost in repairs [1].

1.1.2 Existing sensing approaches

Two main approaches have been commonly taken to develop such systems: (1) fiber-optic sensors and (2) electrical-resistance based sensing devices. However, due to the size limitation on the spectrum scope as well as the required continuous length, it is extremely challenging to fabricate a compact and portable and wireless fiber-optic sensor.

On the other hand, the electrical-resistance based sensor can be downsized, making them ideal candidates for the next-generation wireless sensing platform. However, the commercially available strain sensors cannot satisfy the critical requirement for crack sensing which is to have both the high resolution and large sensing range simultaneously without enlarging the sensor size. The root cause of the drawback was rooted in the basic design of the commercially available strain gages (typically metal foil strain gauge) as illustrated in Fig. 2. By embedding a thin metal coil to the hard polymer substrate, this type of strain gauge relies on the relatively small stretching of the coil segments within each grid length to amplify the changes of electrical resistance. Due to the high sensitivity of metal to straining, a high resolution in terms of strain measurements can be achieved. However, for a relatively large strain, which is often time observed in crack sensing, this design loses it appeal due to the low failure strain of the metal coils.
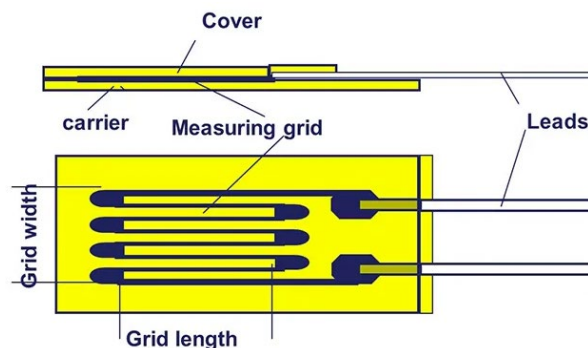
Fig. 2: Design of a typical metal foil strain gage [2].

To overcome this shortcoming, the mechanical sensors have been widely used for crack measurements. One of the most adopted mechanical sensors is the extensometers as illustrated in Fig. 3. These mechanical strain gages utilize levers to mechanically magnify the cracking within the gage length to achieve better resolutions. Although these devices are relatively reliable and have the range of measurements needed, their need for installation and vulnerability to environmental conditions (rain, moisture, and low temperatures) make them impossible for long-term crack sensing and monitoring.
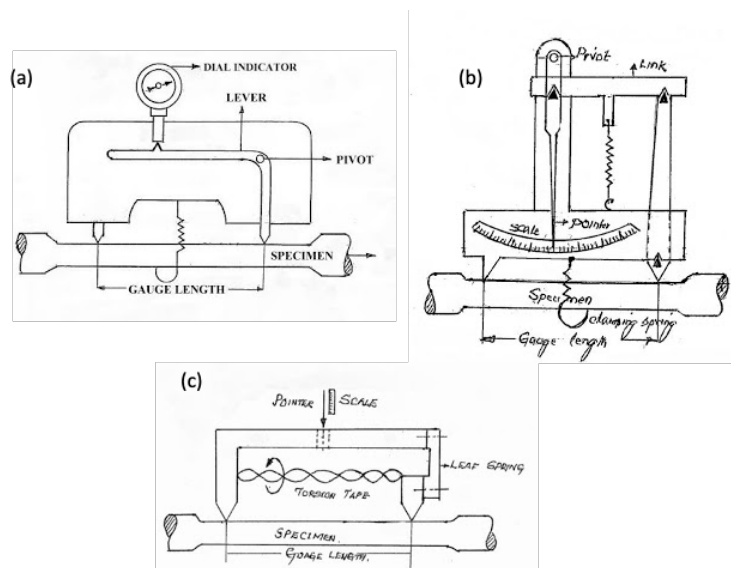
Fig. 3: Design of typical mechanical strain gage (extensometers): (a) Berry, (b) Huggenbeger, (c) Johansson [3].

Certainly, there are other types of crack sensing including the non-contact image-based measurements [4]. However, these image-based methods have high requirements for lighting conditions, surface textures, as well as image acquisition equipment.

1.1.3 Proposed sensing materials and mechanisms

To overcome the challenge to find a new sensing approach for cracks that offers both high resolution and long-range measurements, we turn our attention to the rapidly developed functional soft materials. Active or functional soft materials are often time polymeric composites that have functional fillings to achieve exceptional electrical, optical, or magnetic properties. The early explorations were the combination of carbon black particles deposited on rubbery substrates [5]. However, the relatively large carbon black particles and difficulties of achieving uniform mixes posed challenges in consistencies for large scale applications.

With the rapid growth of nanotechnology, graphene has emerged as ideal material for sensing applications, which has exceptional conductivity, dispersion capability, as well as durability [6]. For the matrix materials, PVDF has drawn a tremendous amount of attention due to its interesting piezoelectric properties. Polyvinylidene difluoride (PVDF) is a thermoplastic polymer with a semi crystalline microstructure and a varied polymorphism, showing high compliance, thermal and chemical stability, and piezoelectric and pyroelectric properties. These properties are the base of different applications such as tactile sensors, infrared imaging devices, actuators, electrolyte-gated transistors, etc. [7]. The incorporation of different nanofillers is a way to further improve the performance of raw PVDF and extend its applications (Fig. 4). In this project, we utilized the graphene as the nanofillers to create the network structure. This conductive network structure offers two sensing mechanisms: (1) the piezoresistive mechanism, where the stretching of PVDF matrix changed the internal contact of graphene flakes leading to changed electrical resistance, and (2) the piezoelectrical mechanism, where the local electrical field generated by the networked graphene structure offered change of resistance as well. We found that the piezoresistive mechanism is dominant due to the almost linear relationship between the straining and electrical resistance, which is convenient for the proposed crack sensing. In addition, the

4

inherently large deforming capability of PVDF offered the possibility for the required large cracking strain.
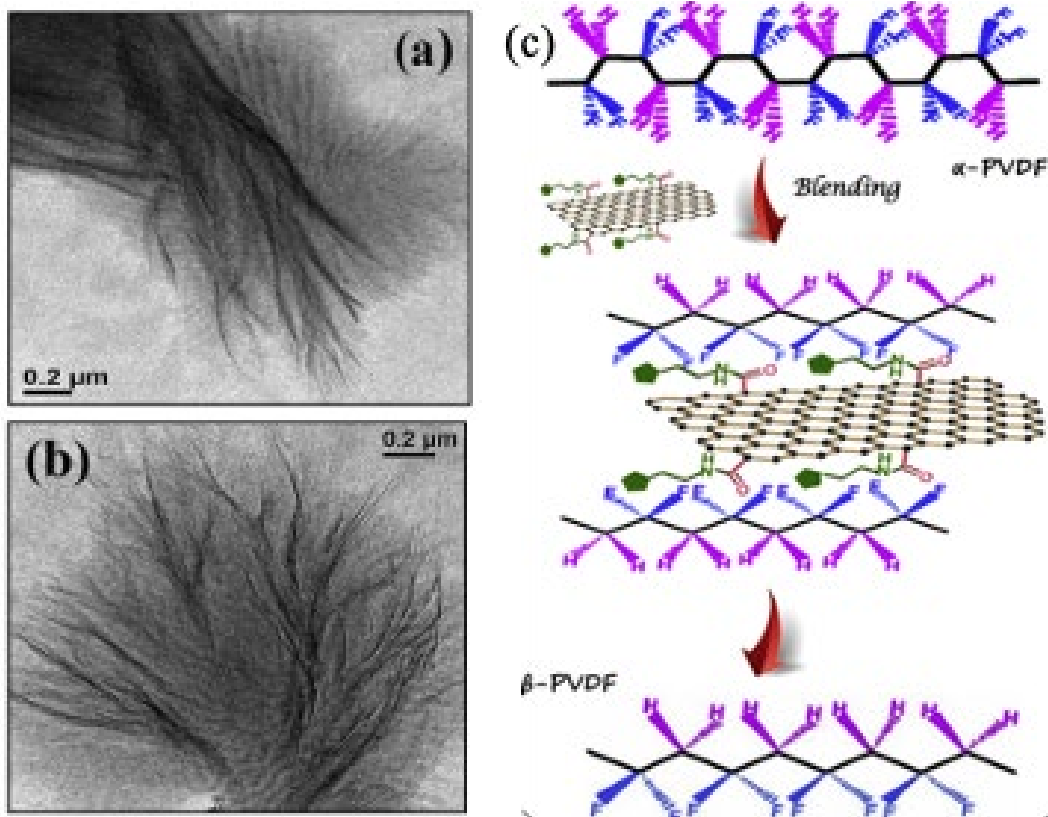
Fig. 4: (a) (b) TEM images of PVDF-graphene with different concentration of graphene oxides; (c) Molecular structures of reduced graphene oxides with PVDF [8]

1.1.4 Data transmission, crack growth warning, and self-efficient energy system

For data transmission system, we needed a portable, integrated computer device that could effectively receive, process, analyze the strain data as well as detecting and tracking the abnormality of the data. The ideal system should also be low cost and low power consumption so that it will be affordable to large scale applications. To achieve this purpose, we selected the recently emerged Raspberry Pi systems [9], which offers both flexibility in integrating data receiving and processing units.

For the data processing, we needed a real-time, automatic "processer", that reviewed the strain data, processed the data, and understood the trend of the data to establish a baseline for normality. Then when an incident (such as sudden crack growth) occurs, this "processer" can detect and send corresponding messages to bridge engineers. For long term monitoring, we cannot rely on a human to process, which could be costly and ineffective. We then sought the help of recently developed machine learning approach to achieve this detection. In this project, we utilized the deep artificial neural network (ANN) approach to establish the data normality. For the case study, we installed the sensing system to the exterior railing of a residential building to understand the thermal straining phenomenon. When an incident such as sudden impact occurs, we observed a sudden increase of strain, which can then be detected by the trained ANN approach. This provided the potential solution to the crack growth warning issue. Finally, we also needed to reduce the entire system to run on a small capacity energy storage device (e.g., a 9-volt battery), which should be able to be charged by a solar panel to achieve self-energy efficiency for targeted long-term monitoring.

1.2. General Approaches, Challenges, Solutions, and Tasks

From the literature study and rationalization presented in Section 1.1, we decided to utilize the PVDF polymer matrix and graphene nanofillers to make the soft piezoresistive sensor, which is capable of large deformations with high strain to electrical signal sensitivity. We also decided to utilize Raspberry Pi devices to integrate the data acquisition, processing, and wireless transmission. We utilized machine learning to further process the data, learn the normal strain variation trend and detect abnormal strain readings. Combining these three techniques, delivered a novel sensing system that can wirelessly sense a crack, detect crack growth, and alert engineers in real time. Despite the promise, there are several critical questions that needed to be answered from the application aspects:

(1) Can we achieve low cost, large scale processing to deliver high quality of graphene needed for the sensor fabrication?

(2) Does the microstructure of the sensor matter in terms of sensing sensitivity? (i.e., is thin-film structure better than the popular core-shell fiber structure?)

(3) What is the optimum percentage of nanofillers we should use to achieve high sensitivity?

(4) Can we achieve portable packaging for the sensing unit with desired data acquisition, processing, and transmission?

(5) Can artificial neural network (ANN) approach understand the relationship between strain measurements and normal load? Can it detect abnormal strain measurement?

Among them, Questions 1-3 are related to the materials and sensor fabrication, which were addressed in **Task 1**. Question 4 belongs to the hardware component, which was addressed in **Task 2**. Question 5 belongs to the data processing software, which was addressed in **Task 3**. The specific contents of these three tasks are summarized below:

Task 1: Materials synthesis, sensor fabrication, and sensor validation

We developed a low cost and efficient way to produce graphene flakes using electrochemical exfoliation method. In addition, we compared the two types of sensors made with two different structures: (1) PVDF-graphene thin film sensor for small cracks; (2) zig-zag shaped sensor with graphene coated glass fiber to cross large initial cracks. We also conducted the validation for the two types of sensors.

Task 2: **Hardware development for data acquisition and transmission**

We developed the Raspberry Pi system and converted the analog signal to digital signal for the ease of data transmission and data precision. We also developed the portable package with solar-panel energy harvesting device for self-efficiency. In the end, we established an online real-time database that allows us to transmit the data using cellular network (4G) and store them in the

cloud server. The cloud server was also able to message other mobile devices if certain abnormality was observed.

Task 3: **Software development including cloud data storage and machine learning for strain data processing**

We developed the online platform for data storage and processing. In addition, we also explored the usage of machine learning to understand the "normal" strain variation and differentiate the abnormal signals from the normal trend. We also validated this approach with a simple case study.

2. RESEARCH PROGRAM

2.1 Task 1: Materials Synthesis, Sensor Fabrication, and Sensor Validation

2.1.1 Materials synthesis

The materials needed in this study were graphene flakes, PVDF polymers, PDMS polymers, as well as glass fibers. To reduce cost, we developed an electrochemical exfoliation process to produce large amounts of graphene sheets with significantly lower cost than the conventional chemical vapor deposition (CVD) approach [10]. The specific details of material synthesis are provided below.

Graphene: In this work, electrochemically exfoliated graphene was synthesized, which have the advantage in low cost and high production. Briefly, Graphite foil (Alfa Aesar, 0.5 mm thick) was cut into 2.5 cm × 8 cm pieces and used as the anode and source of graphene for the electrochemical process, while a graphite rod (Graphite Store, diameter of 24.5 mm) was employed as the counter electrode. 0.1 M solution of ammonium sulfate ($NaSO_4$) was purchased from Sigma-Aldrich and used as the electrolyte in aqueous solution (as shown in Fig. 5a). The working electrode's exfoliation occurs as an immediate consequence of the applied voltage between the two electrodes, for example, +15 V (ISO-TECH IPS-603 DC power supply), which generates a starting current of ~0.4 A. Produced powder was collected by vacuum filtration on PTFE membranes (pore diameter of 5 μm), and after several rinsing steps needed to remove salt residuals, it was dispersed in N,N-Dimethylformamide (DMF) (Sigma Aldrich) by mild sonication for 20 min (as shown in Fig. 5b). Using DMF as a solvent helped avoid the aggregation of graphene. Such dispersion was kept decanting for 48 h to promote the sedimentation of unexfoliated material. After that, supernatant solution was taken as monolayer graphene dispersion. The lateral size of monolayer graphene is ~ 1μm. The filtration process was repeated, and the collected monolayer graphene was dried in a vacuum oven overnight for future use.

PVDF matrix materials: Polyvinylidene fluoride (PVDF) has unique properties such as highest chemical resistance, high temperature sustainability, and it has been applied in a wide variety of fields such as piezoelectric, pyroelectric, etc. In this work, PVDF with molecular weight of 100000 g/mol from Alfa Aesar was utilized for the matrix material for the sensor.

PDMS sealant materials: Polydimethylsiloxane (PDMS) Sylgard 184 was purchased from Dow Corning. PDMS preparation procedure was as follows. Firstly, we mixed the PDMS and curing agent with weight ratio of 10:1. Secondly, we degassed the mixer to remove bubbles. After pouring to the area needed, the PDMS sealant was cured at 70 °C for 0.5 h.
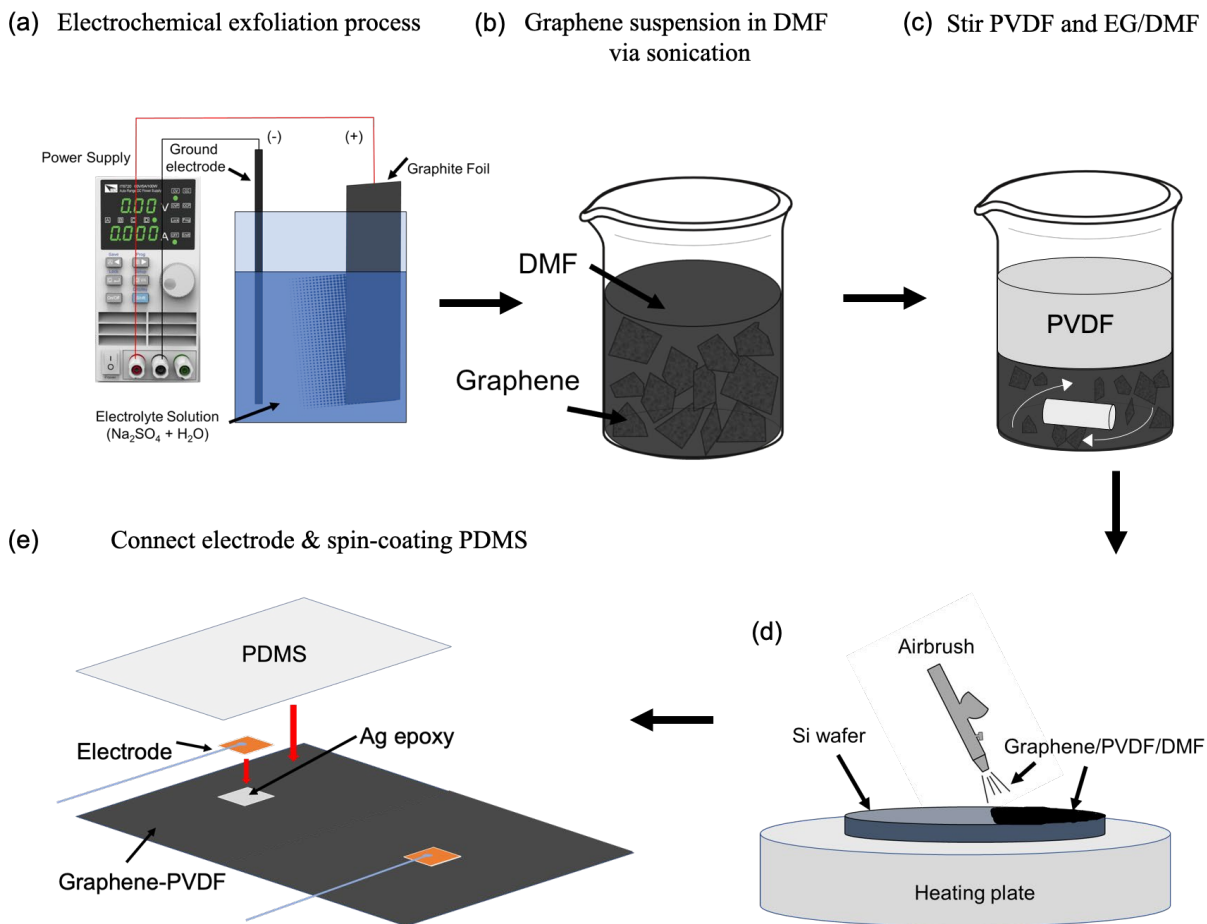

Fig. 5: (a) Synthesize electrochemically exfoliated graphene, (b) disperse graphene in DMF, (c) mix PVDF and graphene in DMF, (d) spray PVDF/graphene to Si wafer and (e) connect wires and coat PDMS protection layer.

2.1.2 Sensor fabrication

Two types of sensors were fabricated including the PVDF/graphene thin film sensor for the small cracks and the graphene coated fiber sensor for large cracks. For the PVDF/graphene thin film sensor, graphene was mixed with PVDF first to form a thin layer then packaged with PDMS sealant layer with electrodes embedded in the PVDF/graphene layer. For the fiber sensor, the graphene was firstly coated on top of glass fiber, then the coated fibers were bundled and glued to the surface for crack detection. The fabrication details are described below.

PVDF/graphene thin film sensor for small cracks: To prepare PVDF/graphene nanocomposites with different weight fractions of graphene, the procedure is as follows. Initially, a fixed amount of graphene was dispersed in DMF by sonicating for 60 min. Meanwhile, a fixed amount of PVDF polymer was dissolved in DMF with the help of a magnetic stirrer for 30 min. Then, these two solutions were mixed by sonicating for 1 h, followed by magnetic stirring (as shown in Fig. 5c). The mixed solution was sprayed onto a Si wafer using an Airbrush (Master Airbrush) as shown in Fig. 5d. The nozzle size was 0.5 mm, and the operating pressure is 80 psi. To increase the hydrophilicity of the Si wafer surface, firstly, Si was cleaned by soaking it in acetone at 55 °C, followed by rinsing in methanol and distilled water; then, the Si wafer was soaked in piranha solution (vol. ratio 3:1 of H_2SO_4 and H_2O_2) for 6 h. After slowly evaporating DMF solvent at 50 °C, PVDF/graphene film was peeled off from the Si wafer and cut into the needed shape using a cutting machine (Silhouettes). Cu wires were bonded to both sides of the PVDF/graphene film using Ag paste, which helped reduce contact resistance. At last, PDMS, which acted as a protection layer was spin-coated onto both sides of PVDF/graphene film respectively (2000 rpm for 30 s) and cured (as shown in Fig. 5e).

Fiber based zig-zag sensor for large cracks: To improve the adhesion between the graphene glass fibers, the fiber surfaces were chemically treated and exposed to oxygen plasma.

11

At first, glass fibers were heat treated at 600 °C for 1 h in a box furnace (Thermal Scientific) to remove residual coating on fibers from the commercial manufacturing process. Next, fibers were treated in Piranha solution for 10 min followed by washing with DI water to make the surface more hydrophilic. To coat the glass fibers with electrochemically exfoliated graphene, firstly, 10 mL of aqueous graphene solution (3–5 mg/mL) was poured into a plastic weighing boat (10 cm diameter). After that, surface treated glass fiber bundles were dipped into a graphene in DMF dispersion, which contains monolayer graphene, for 5 min followed by drying in air for 5 min (as shown in Fig. 6a). This process was repeated with varying number of dips with a range of 5, 20, and 50 dips. The glass fiber with graphene coating is shown in Fig. 6b.
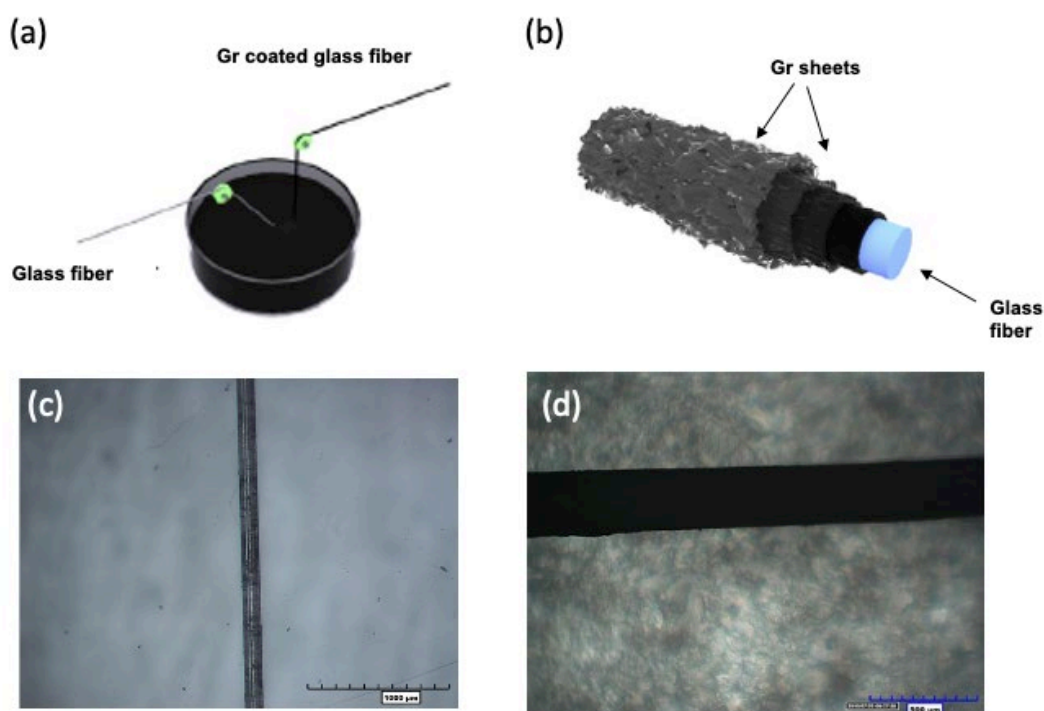
Fig. 6: (a) Coat graphene onto glass fiber surfaces, (b) the graphene coated glass fiber structure, (c) optical image of single glass fiber coated with graphene, (d) bundle of coated glass fiber.

2.1.3 Sensor validation

For PVDF/graphene composite, two variables that were noticed to affect the film resistance during the manufacturing process, were graphene concentration by weight and the stirring time of the PVDF/graphene mixture. The experiment set up, as shown in Fig. 7a, was used to study how these two factors influence the film resistance. Multiple PVDF/graphene composites with graphene concentration in weight range from 1% to 9% were prepared and the resistance of each film was recorded as shown in Fig. 7b. It was found that with the increase of graphene concentration, the film resistance decreased. However, the decreasing resistance terminated at 50 $k\Omega$ when the graphene concentration arrived at 8%, which indicated the effect of graphene on increasing conductivity was saturated (shown in Fig. 7c). The graphene with 8% concentration was used to determine the effect of stirring time of PVDF/graphene inside DMF on film resistance. Solutions were stirred from 1 – 25 hours at 2500 rpm using a magnetic stirring stick.

Fig. 7: (a) Experiment set up for resistance measurements, (b) average resistance versus graphene concentration, (b) average resistance versus stirring time.

To calibrate the PVDF/graphene composite used as a strain sensor, the composite was bonded onto an aluminum with a pre-crac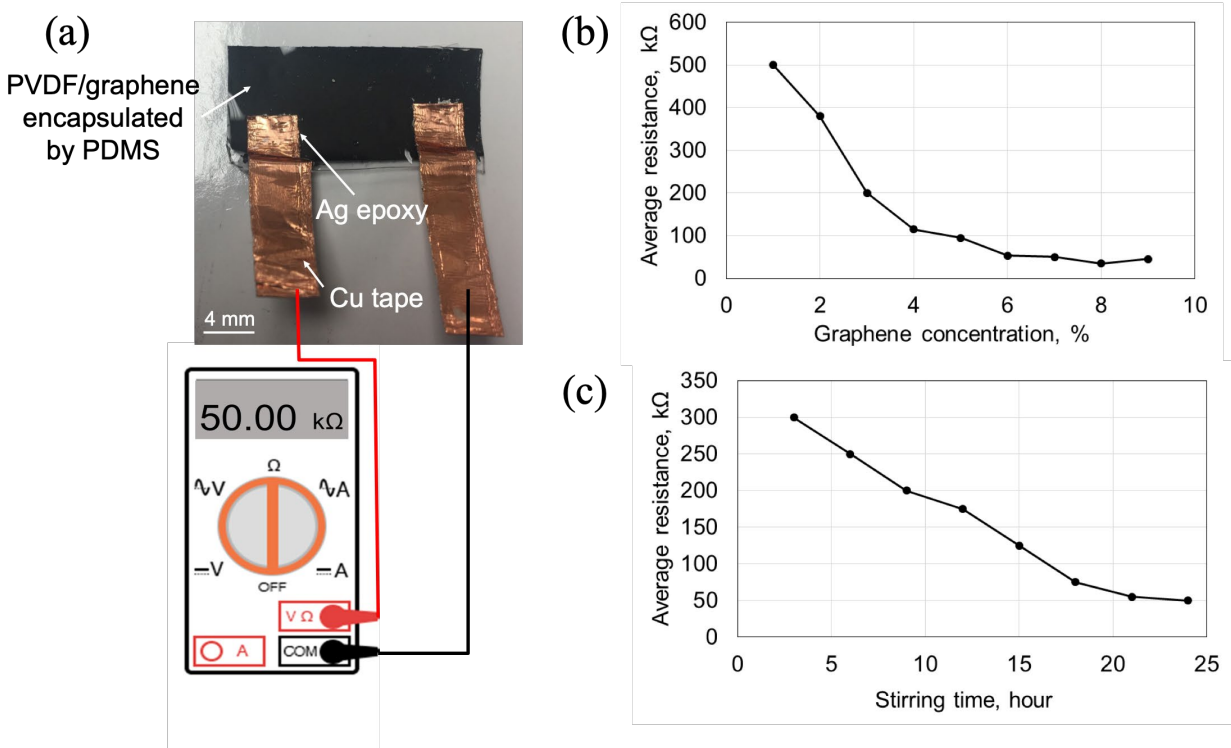k in the middle. Then the aluminum plate was loaded in the Instron Testing Machine for tensile testing as shown in Fig. 8a. Load *versus* displacement curve was obtained from Instron and load *versus* strain at PVDF/graphene bonded area was calculated. At the same time, the resistance values of PVDF/graphene composite were also recorded by a National Instruments Data Acquisition system with the composite in a quarter Wheatstone bridge configuration. The results were shown in Fig. 8b and the gauge factor was calculated to be 20 using the equation $\frac{\Delta R/R_0}{\varepsilon}$, where ΔR is resistance change, R_0 is initial resistance, and ε is strain. Then, in the application, the strain could be calculated when the $\Delta R/R_0$ is measured.
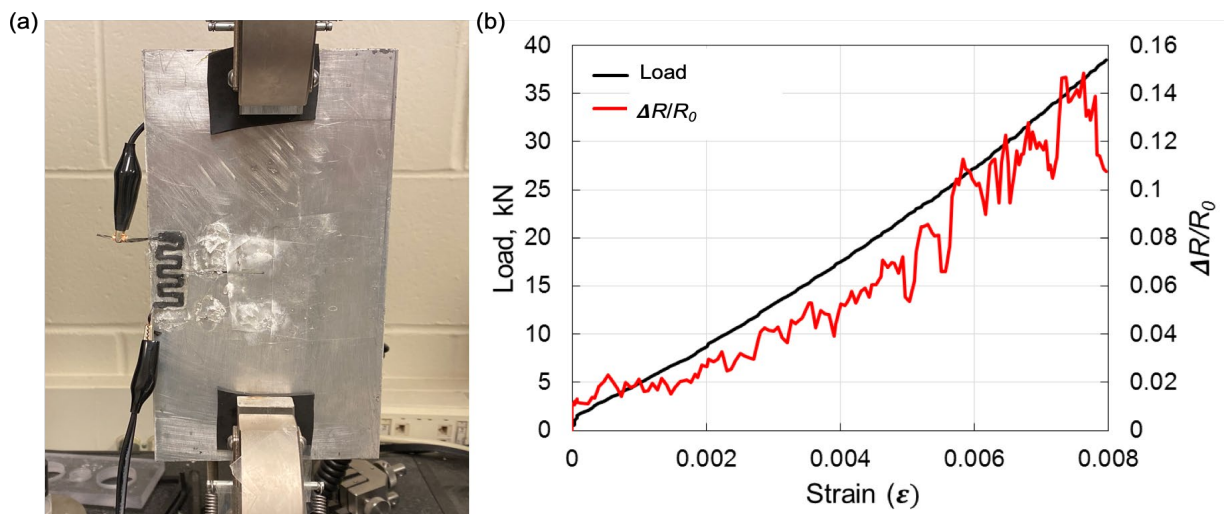
Fig. 8: (a) Experiment set up for strain sensor calibration, (b) load versus strain and ΔR/R_0 versus strain.

Due to the limitation of glass fiber length and resolution of strain measured, a micro tensile tester was used to do calibration of the graphene coated glass fiber. Cu films were glued to the edges of the glass fiber to avoid slip between clamps of the micro tensile tester and the glass fibers. Similarly, force *versus* strain and $\Delta R/R_0$ *versus* strain curves were obtained and shown in Fig. 9.

14

The gauge factor was calculated to be 5, which indicated the graphene coated glass fiber has less sensitivity than PVDF/graphene composited when used as a strain sensor.
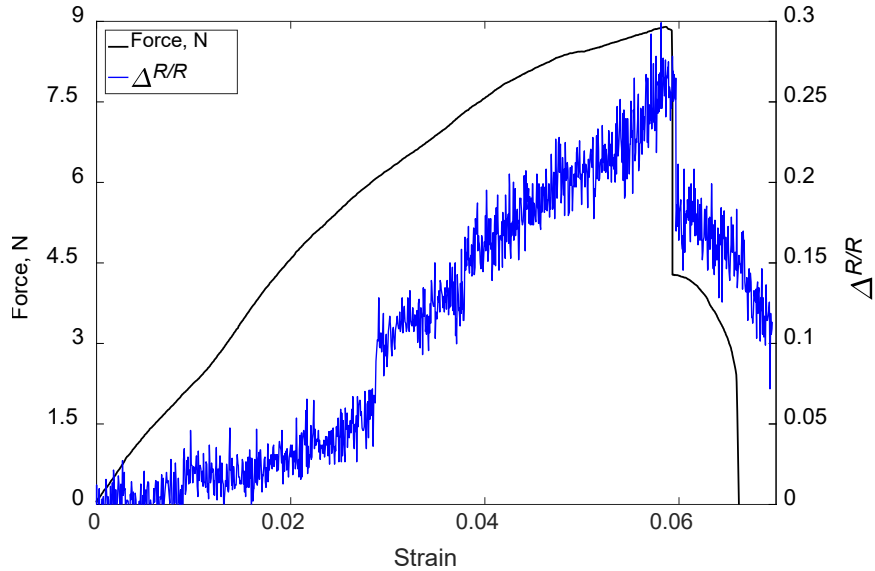
Fig. 9: Force *versus* strain and Δ*R/R_0 versus* strain.

From the sensor validation experiments conducted, we have validated that the sensor can provide high sensitivity in terms of straining. The limit of detection for the strain was found to be about 1×10^{-4}, which is comparable to the commercially available metal coil type strain gage. However, the range of measurements (total stretching of the sensor) was about 200% of its original length, far exceeding any commercially available metal coil type strain gage. These results demonstrated that the developed nanocomposite sensor can satisfy the required strain measurements.

2.2 Task 2: Hardware for Data Acquisition and Transmission

2.2.1 Arduino and Raspberry Pi

In this section, we discussed the two data acquisition systems in conjunction with the sensors developed: (1) the Arduino DAQ system, and (2) the Raspberry Pi system. We utilized the Arduino DAQ system first since it was readily available in the lab and has exhibited excellent performances

for some of our other sensors [11]. In addition, we preferred its on-board Bluetooth transmitter, which can help pass the data directly to our mobile computing devices. The layout of the Arduino system utilized in the calibration of our prototype sensors is shown in the Fig. 10 below.
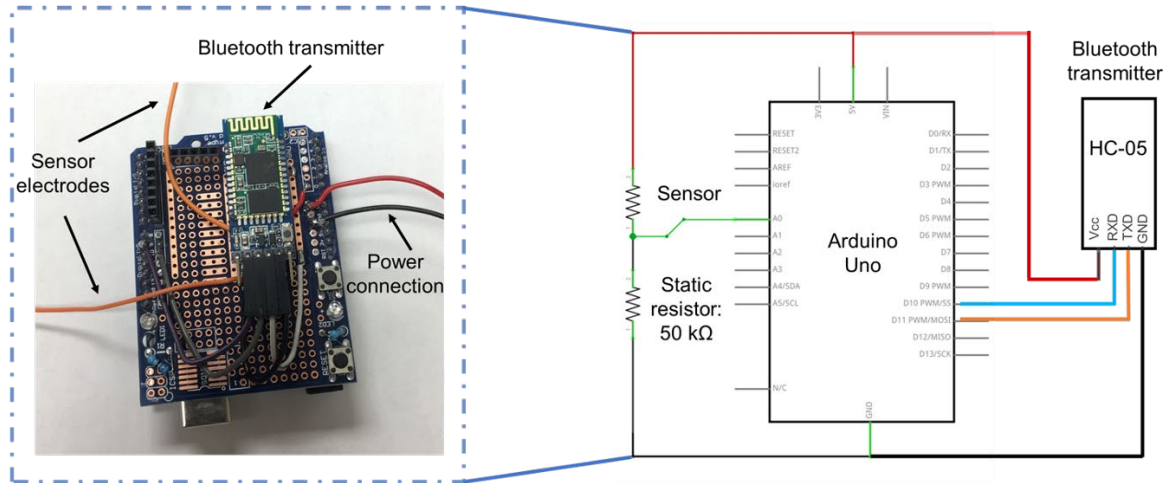
Fig. 10: Arduino DAQ system built and utilized for our prototype sensor calibration.

In the Arduino DAQ system, the crack/strain sensor works as a potentiometer in the system where their changing resistance was measured against a constant resistance. However, we soon realized that there are several disadvantages using the Arduino DAQ system: (1) the signal output is 10-bit resolution, which gives steps of 4.88 mV, which is too coarse for fine strain readings; (2) the Arduino DAQ system needs separation components that work with it to achieve other functions including data transmission via cellular network, solar power management system, video recording capability, as well as analog to digital conversion.

Based on these limitations, we selected the Raspberry Pi system (Pi system for short). Taking advantage of the flexibility of the Pi system, we were able to have the following new features. (1) We were able to transmit data via 4G cellular network. This feature allowed the data to be transmitted in long range to remote servers. This feature also allowed the server to directly

receive .txt files and store them, which accelerated the data processing and message sending. (2) A solar power management system was successfully built and incorporated using the Pi system. This was crucial since we needed to manage the power consumption to achieve long-term monitoring reliability. For instance, with the Pi system, we have successfully demonstrated that we can utilize 9Ah battery maintained by a 6W solar panel for continuous power supply. The specific power management strategies we explored were: (i) dynamic control of sampling rate, and (ii) periodic shut-down and activate the system. (3) The Pi system allows video feed, which allows future surveillance and inspection of infrastructure. In addition, we explored the usage of a 5 Megapixel camera, and up to 1080p@36fps with a 20-180° field of view. However, due to the limitation of the scope, we did not include the details of video feed in this research. (4) Finally, the Pi system had a convenient 16-bit resolution analog to digital converter as illustrated in Fig. 11a. With this digital conversion, we obtained a more precise strain data collection.

2.2.2 Standalone system

Specifically, we showed the Pi-integrated sensing system (only sensor and DAC) is highly portable, and that we can enclose the system to be within a water-proof box with a 9 V battery inserted as illustrated in Fig. 12. It should be noted that each DAC system can handle 8 sensors sensing and recording simultaneously. To extend the field life of the sensing system, we also equipped the sensing system with a solar power system and a charge regulator as illustrated in Fig. 13. This solar powered system was finalized and recommended for field implementation.
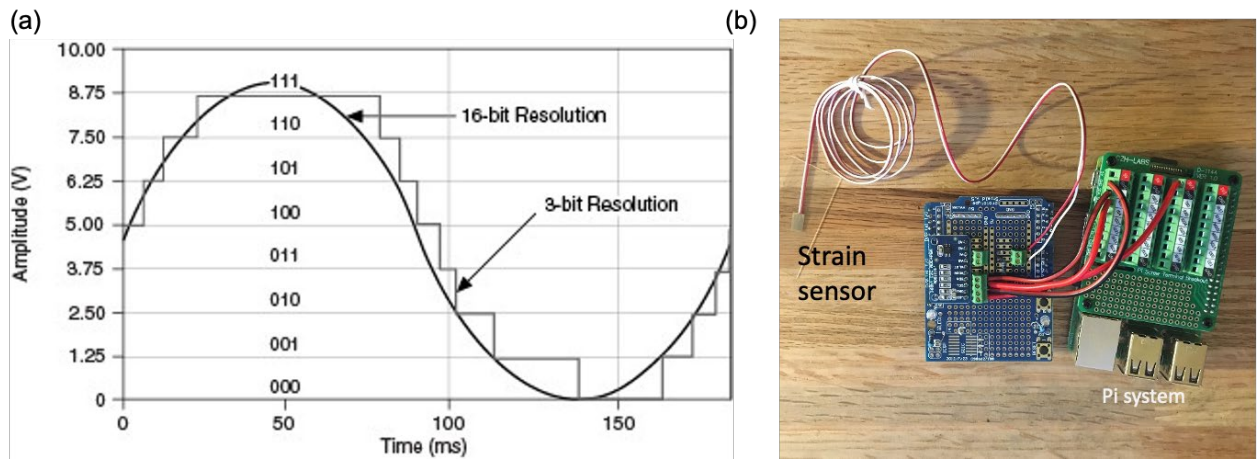
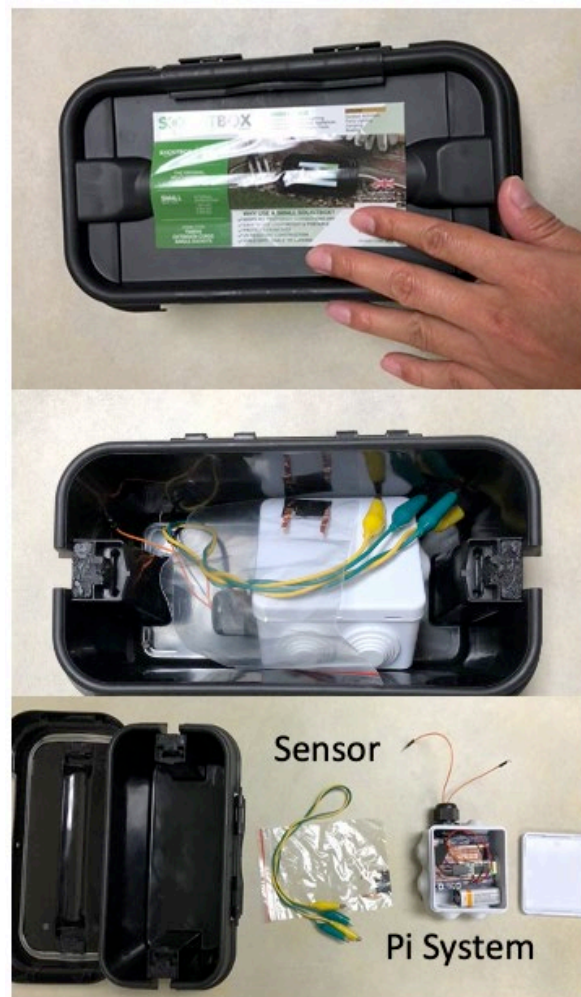**Fig. 11:** (a) Illustrative comparison of 16-bit and 3-bit resolution, (b) sensor with Pi system

Fig. 12: Potable sensing system

System Overview

Solar Panel

Power Management Box

Power Management Box

Input Power from
Solar Panel
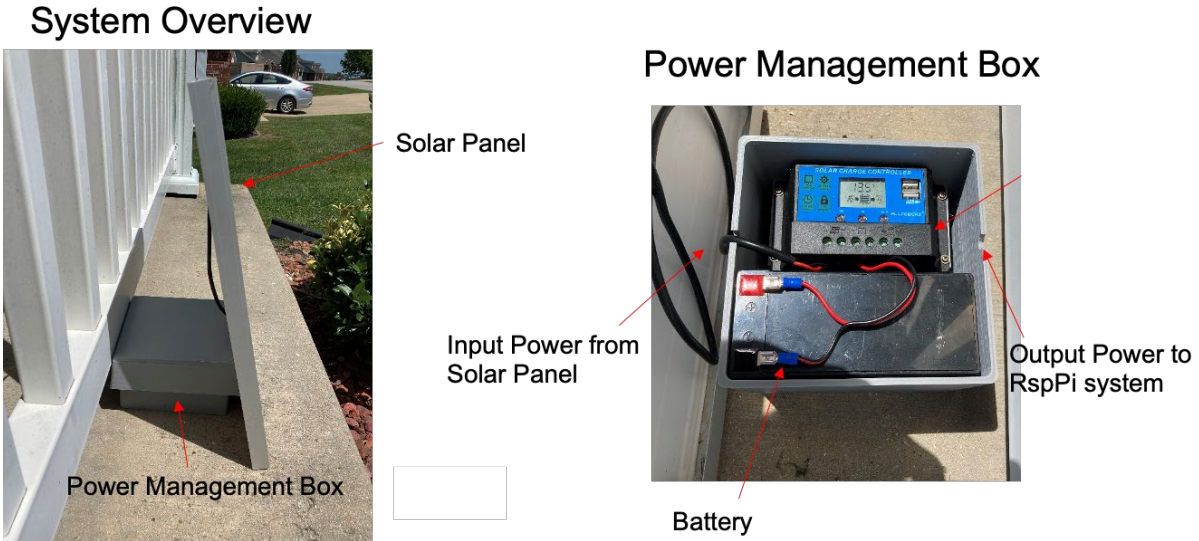
Output Power to
RspPi system

Battery

Fig. 13: Sensing system with solar power integrated

2.3 Task 3: Software Development Including Cloud Data Storage and Machine Learning

2.3.1 Data transmission and cloud storage

With the hardware completed, we then built the cloud data storage, transmission mechanism as well as the machine learning assisted data processing algorithm. The data collected from the Pi-system was uploaded to the cloud through the cellular 4G network. The team made inquiries to the local wireless communications service providers (ATT and T-Mobile). The cost of each data transmission line is about $15-$25 (no images), which is sufficient for more than 100 sensors if data management is implemented (dynamic scanning rate). For a server, we utilized the on-line free service from Google Firebase Realtime Database [12].

We tested our system working with the server. The preliminary data transmitted to the server using the temporary sim card are plotted in Fig. 14. It should be noted that the web app was programmed to display these data in the real-time, which can also be sent to cellphones or other mobile computing devices in real-time.
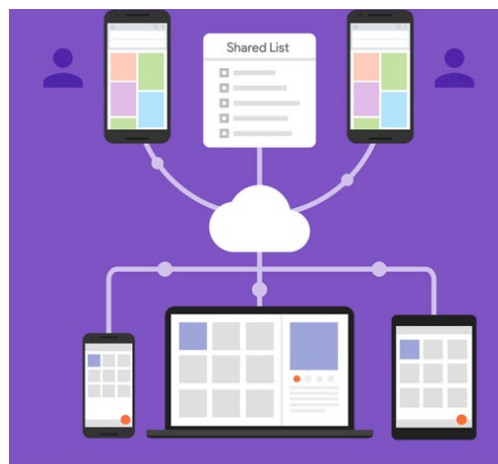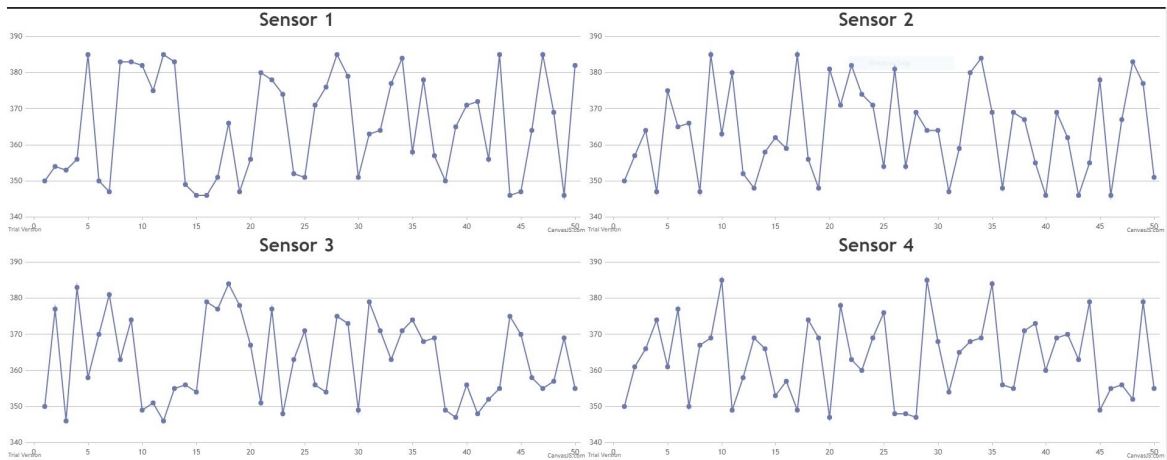
Fig. 14: (Top panel) Sensing data uploaded to server and displayed on web app in real-time: x-axis is time in hour, y-axis is the resistance readings in ohm; (bottom panel) cloud data service by firebase.

For the preliminary test, the strain/crack sensors were attached to the railing of the residential building as illustrated in Fig. 15. From the sparse data displayed in Fig. 14 (which is adjustable by using different scanning rate), we found significant fluctuations of strain data with respect to time. It is suspected that the sensors are sensitive to thermal fluctuation, periodic local vibration, as well as other disturbance. This complex environmental loading, especially the thermal

20

effect, should be excluded when judging the abnormal strain increase possibly due to excessive structural load.
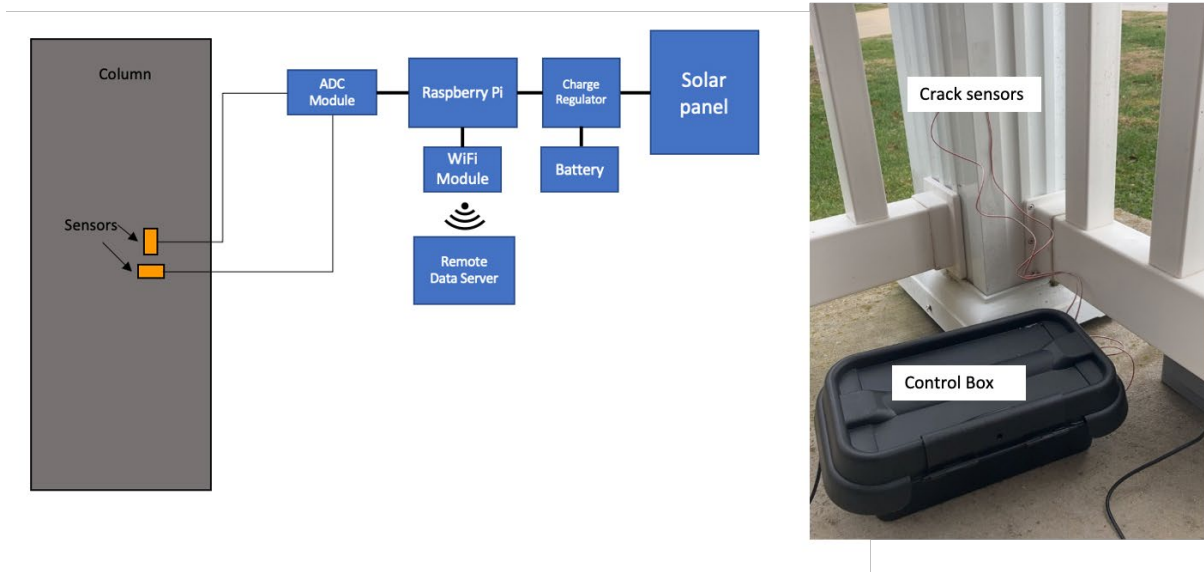
Fig. 15: (Left panel) illustration of sensing system, (right panel) sensor installation location with control box nearby.

2.3.2 Machine learning understanding thermal straining and abnormal signal detection

Thermal strain is a critical aspect in structural engineering. Several research projects have been conducted in correlating temperature with the strain reading. However, most of these works focus on eliminating thermal expansion of the sensor, i.e., strain gauges themselves. Very few works have been conducted to understand the effect of temperature on structural loading and response. Yet, tremendous number of structural failures can be directly related to thermal cycling. Perhaps, the actual reason behind this scarcely investigated issue is its complexity in nature. The coupling between the change of boundary conditions and thermal cycles, which is the cause of the structural loading caused by thermocycling, is almost impossible to decipher. In this work, we utilized a deep learning neural network model to extract this coupled relation and used it in an

analytical model to predict the behavior of the structures only using experimental data. This experimental data came from active monitoring systems measuring thermal strain on members over time. Using these systems with deep learning methods allowed us to determine the structural condition of infrastructure more accurately.

Strain data was collected from an aluminum support column for a railing assembly and awning. Two set of strain gages were placed on the column on opposite sides to classify the type of stress the column is under (tension, compression, or combination). The strain gages in each set were installed perpendicular to each other to collect a strain value in both the x and z direction. Strain data was collected from the gages using a Raspberry Pi 3 B+ with a 16-bit analog to digital (ADC) board which allowed the Pi to understand the analog signals. The testing setup and DAQ system is presented in Fig. 15. Data was collected each hour measuring 10 strain data points and the current temperature. All the data was backed up to a database in Google Firebase. The strain data points for each temperature were averaged to produce a model of the temperature vs strain relationship. Another test was conducted in which an external strain was applied to cause a disturbance in the data.

The data from these tests was initially simulated using the 'sklearn' and 'mpl' neural network packages in Python to simulate supervised learning techniques. This method was replaced with using MATLAB's neural networking toolbox as the Python program was not accurate enough with the amount of collected data points. Data fitting and prediction functions were used in the MATLAB toolbox to create data plots of input, output, and test point plots along with their error. Fig. 16 presents the work schematics followed to find the desired relationship. Both the Python and MATLAB programs used in the experiment can be found in this section.
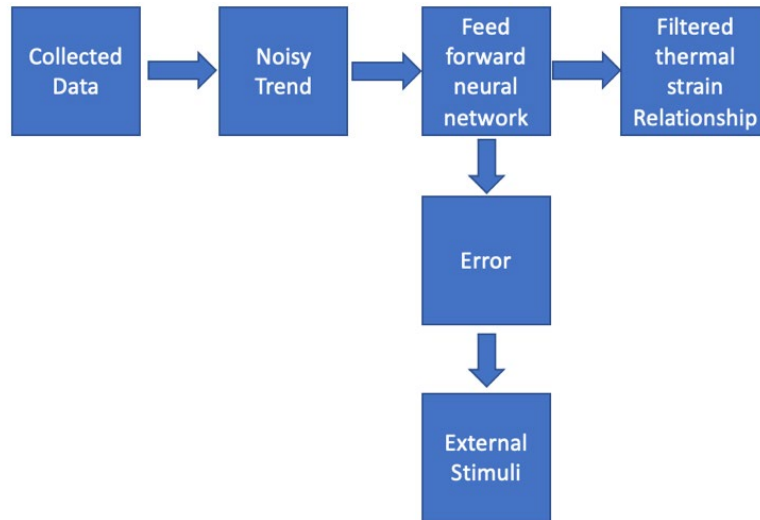
Fig. 16: Workflow scheme followed to develop relationships

The first simulation conducted in the experiment was with a Feed Forward Neural Network with 10 hidden layers. The Levenberg-Marquardt method was used to train the network and its performance determined through mean squared error. The neural network and its structure can be seen in Fig. 17. Fig. 18 presents the structures of the neural network used with the input being temperature and the output being strain. From the fit plot in Fig. 17, some initial error in the training targets can be seen as the fitting curve stays more linear rather than fluctuating with the input data. This behavior reflects into the test targets and outputs with errors on each point averaging approximately 1.625 ohms. Since strain gages are highly sensitive, the goal was to lower this error as much as possible to lower than 1 ohm to ensure accurate prediction capabilities. In Fig. 19, the networks performance of training, test, and validation data points is presented. Using 10 hidden layers, the network had its best validation performance of 2.1628 at its 4th epoch. As shown on the plot, after 10 epochs, the validation performance does not reach an equilibrium level indicating some fluctuations in the accuracy of the network.
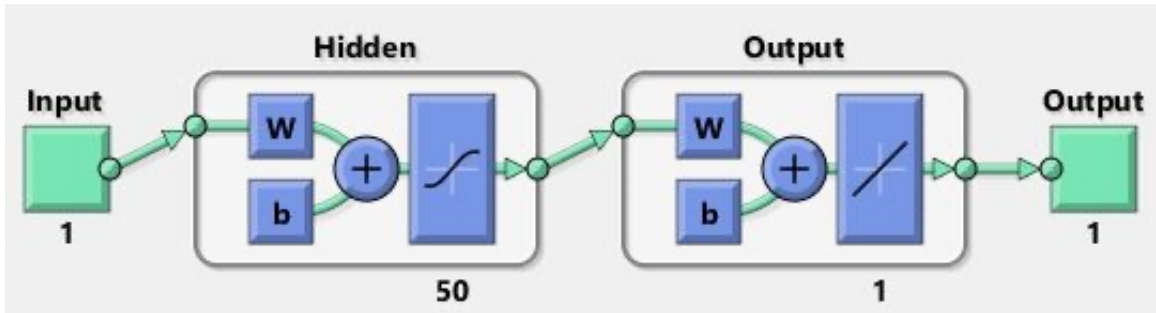
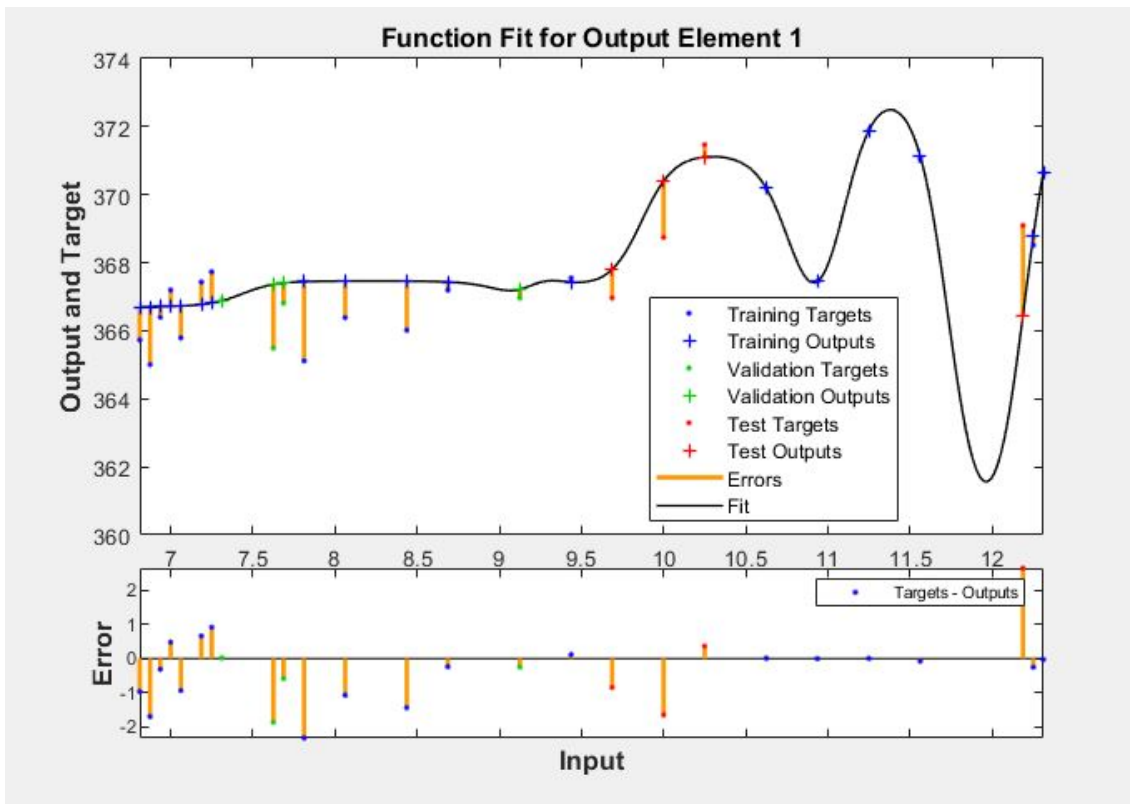**Fig. 17:** Feed forward neural network structure

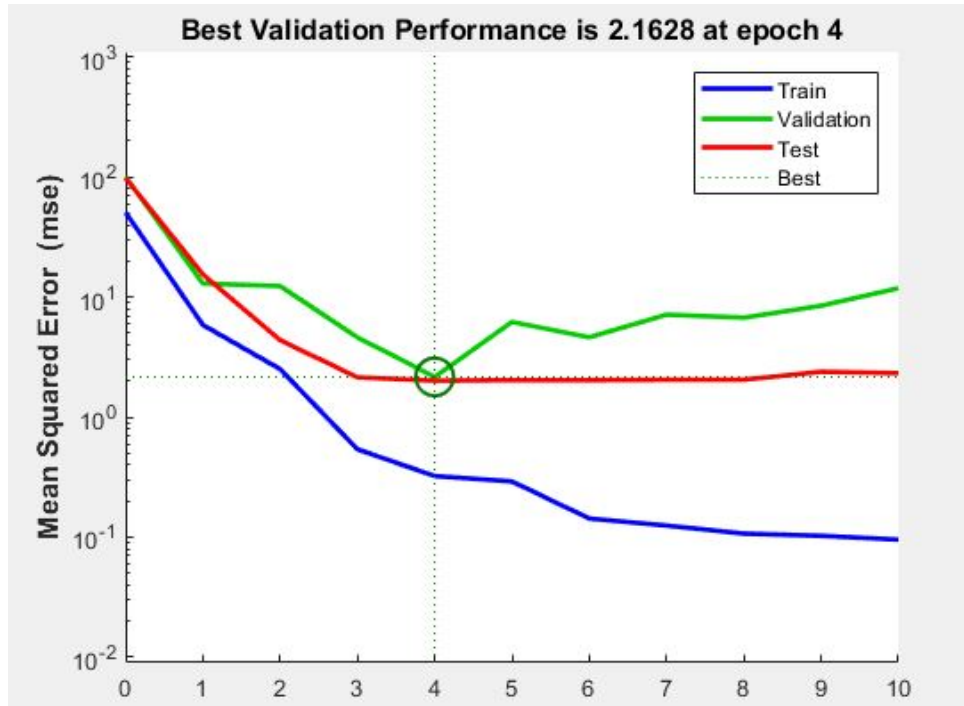**Fig. 18:** System fit of network with 10 hidden layers

Fig. 19: Performance results of network with 10 hidden layers

Further simulations were conducted for the system by increasing the number of hidden layers in the network. Figs. 20 and 21 present the systems fit and performance after being simulated with 50 hidden layers in the network. Looking at the fit in Fig. 20, the system has more fluctuations but has little to no errors regarding the training data. This behavior reflects into the test data points with an average error of 0.875. Increasing the number of hidden layers allowed the system to reduce the error in training and test inputs but did see a slight increase in the validation errors when compared to the network with 10 hidden layers. The performance of this network showed to stabilize much quicker than the previous test and have a significantly larger performance of 10.4865 at its second epoch. This increase in performance can be linked to the networks increase in hidden layers and being able to process these data points through 5 times more layers. Along with this, training, test, and validation data points were all able to come to an equilibrium efficiency

equal to or less than 1 creating stability in the prediction of data points. This stability is important

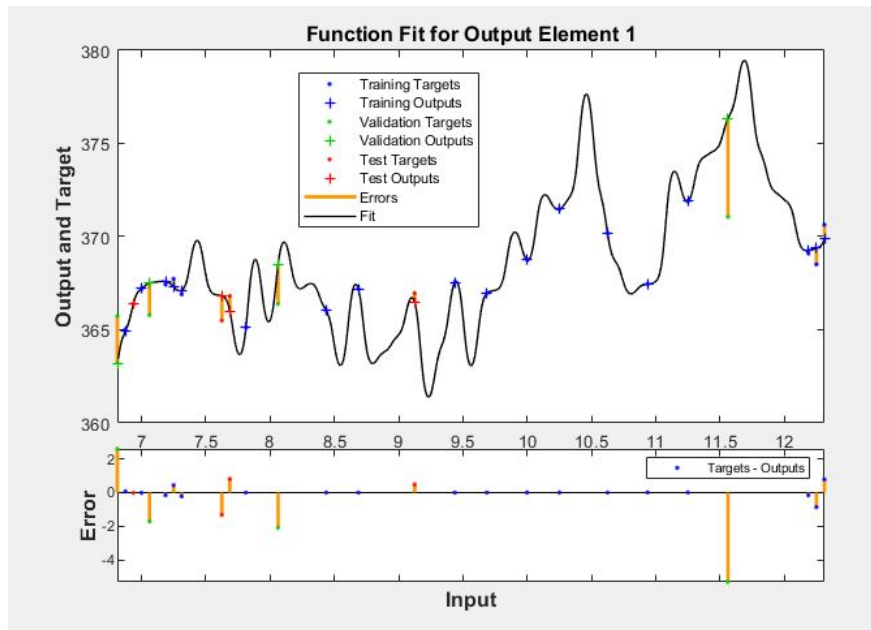in being able to properly understand and calibrate the output of the system.

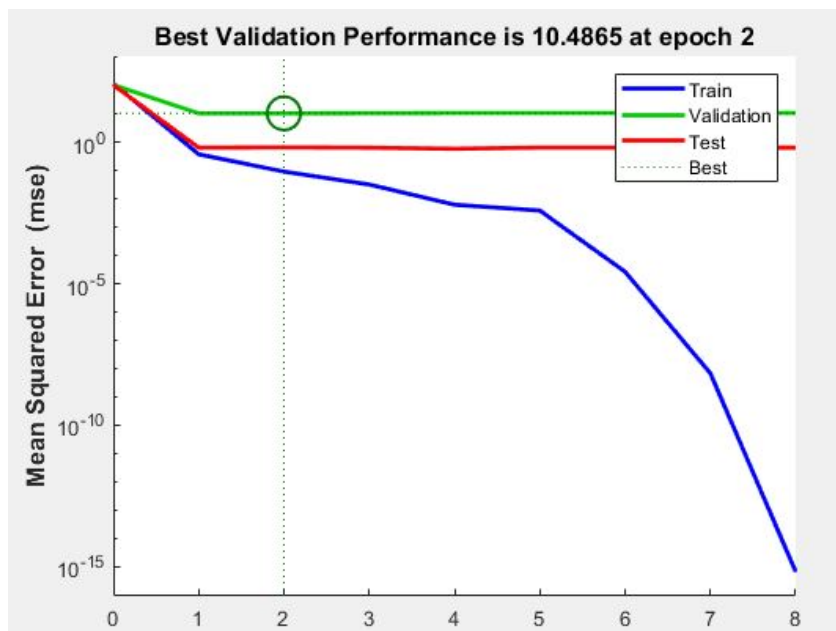**Fig. 20:** System fit of network with 50 hidden layers

Fig. 21: Performance results of network with 10 hidden layers

The final simulation ran was to reflect the system with disturbances included as shown in Fig. 22. Disturbances in the system can indicate large induced loads from an external source. Data from these disturbances provide valuable information in analyzing the structural loading and condition of the members. The disturbance in the data set provided the system with a larger outlier and impacted its performance. Testing various numbers of hidden layers, a total 25 proved to create the best fit with the smallest errors. With the disturbance in the system, the network compared the thermal strain values to the external loads. In Fig. 22, the fit of the system with a disturbance located at 9.25 is shown. The fit line follows the training data points to develop a temperature relationship and has a large error spike at 9.25. This is due to the system expecting one value along the temperature fit and getting a much larger value from the disturbance. Having this larger outlier has impacts on the errors elsewhere in the systems predictions and stability. Although the system had a larger error, knowing where the disturbance is and how it impacts the system is crucial in being able to analyze pure thermal straining. Along with this, being able to detect disturbances in the DAQ system can provide valuable feedback to pinpoint their time and locations. Using this information, a more accurate representation of the strain field on structures was developed.
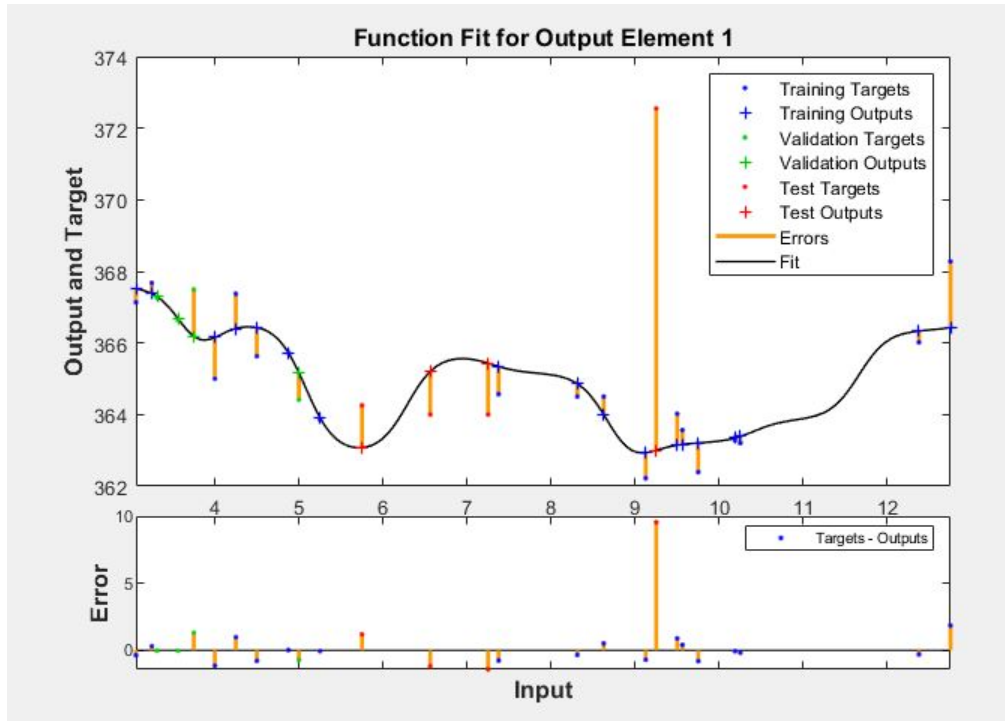
Fig. 22: System fit of network with 25 hidden and included disturbances

Strain data was collected for different temperatures to develop a profile for thermal cycling on the structural members but proved to be less stable than initially predicted due to external stimuli. A feed forward neural network was used to simulate the data collected from the test with temperature being the input and strain being the output. One simulation used a network with 10 hidden layers to develop a relationship and had an average error of 1.625. From the simulations with a network of 50 hidden layers a relationship was created with an average error of 0.875 (Ω). This showed that the neural networks performance had a strong dependency on the number of hidden layers. Another simulation was conducted with large stimuli added and the system was added followed the temperatures trend with a large, detected error at the spot of stimuli. This indicates that using neural networks can be used to detect external stimuli and use it as a filtering effect to study thermal strain cycles. From this study, it was determined that deep learning and supervised learning techniques can be used for structural monitoring of infrastructure with

28

complex loading fields to detect abnormalities. The Python and MATLAB codes are listed in the

Appendix section.

3. RESULTS & DISCUSSION

We would like to discuss the results from the research program by answering the critical questions raised in the introduction section.

(1) Can we achieve low cost, large scale processing to deliver high quality of graphene needed for the sensor fabrication?

The answer is yes. The electrochemical exfoliation method developed in this study produced good quality graphene. We have compared the Raman spectroscopy data and found the characteristic 2D and G peaks as normally observed for CVD (Fig. 23) produced high quality monolayer graphene (Fig. 24).
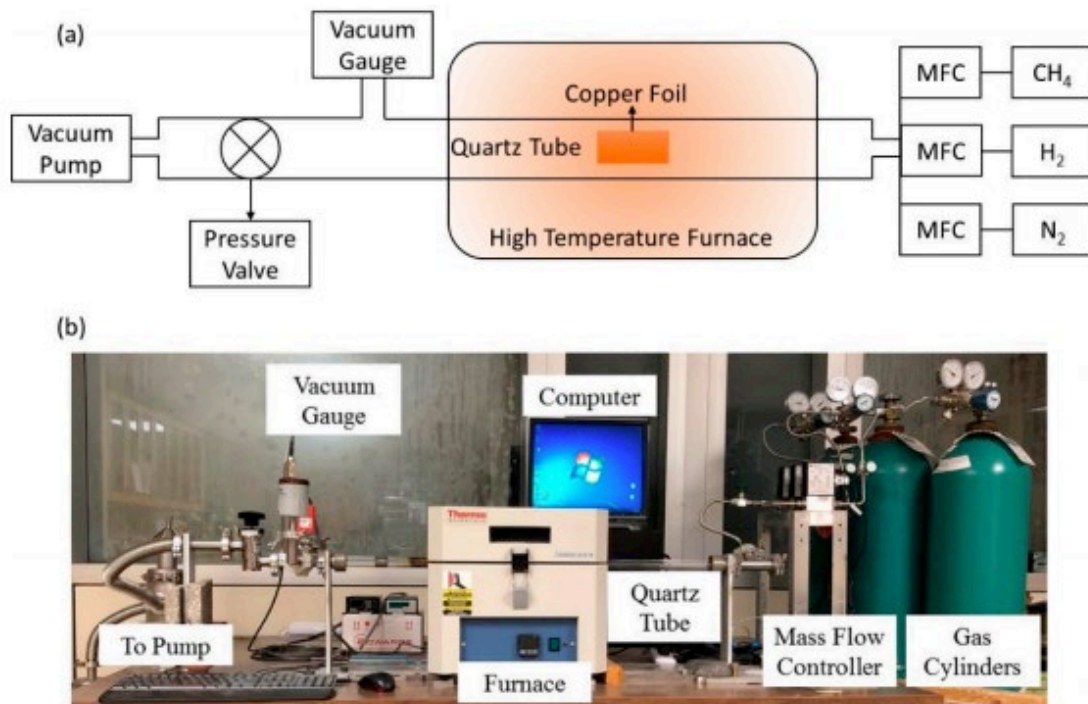

Fig. 23: (a) Schematic illustration and (b) setup of the low-pressure chemical vapor deposition system, MFC, mass flow controller for graphene growth [13].
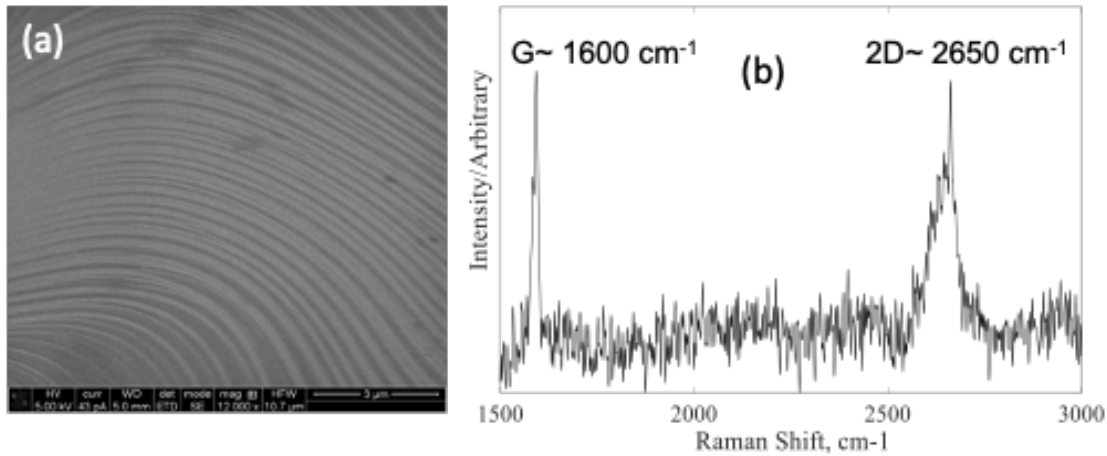
Fig. 24: (a) Monolayer graphene on copper substrate and (b) Raman spectroscopy of

monolayer graphene

These results give us high confidence of utilizing graphene to fabricate large quantities of

the sensors, since the converted price for the electrochemically exfoliated graphene is below 1

dollar per gram. It should be noted that, 1 gram of graphene could be utilized for more than 10

sensors, which lends us confidence for even larger scale applications.

*(2) Does the microstructure of the sensor matter in terms of sensing sensitivity? (i.e., is thin-
film structure better than the popular core-shell fiber structure?)*

Both thin film and core-shell fiber sensors work very well for small and large cracks. The

sensitivity is almost the same. However, for the glass fiber sensor, the measurements range varies

depending on the zig-zag shape and the number of fibers in the bundle. By allowing the fibers to

slip onto each other, we could achieve a longer range of measurements. By increasing the number

of folds in the zig-zag pattern, we could also increase the range of measurements. However, the

durability of the fiber sensor is still a question. Under environmental exposure, the loosely coated

graphene flakes could be debonded from the fiber due to thermal strain and abrasion at the

31

sensor-object interface. Therefore, additional research is needed to evaluate the durability of the sensors.

(3) What is the optimum percentage of nanofillers we should use to achieve high sensitivity?

Approximately 8% concentration was found to be the best filling ratio. When exceeding this value, we found that the electro-resistance of the PVDF/graphene thin film does not change significantly anymore, which indices excessive contact had been established within the graphene network structure. Beyond this threshold, nonlinear relationship is expected between the sensor straining and resistance change.

(4) Can we achieve portable packaging for the sensing unit with desired data acquisition, processing, and transmission?

Yes. We have successfully integrated the sensor with compact Pi-system and a 9V battery that can collect, process, and transmit data to the cloud server using cellular (4G) network. The entire system can fit into a palm size waterproof box. To allow continuous monitoring, we also equipped the system with a solar panel and charge regulator which can be stationed nearby the bridge site. One station can safely handle more than 100 sensors provided a dynamic scanning rate is allowed to minimize energy consumption.

(5) Can artificial neural network (ANN) approach understand the relationship between strain measurements and normal load? Can it detect abnormal strain measurement?

Yes, but not completely. The current results showed that the supervised neural network can learn the thermal strain fluctuations coming from the real-world experiment. It also detected sudden changes from strain readings due to a disturbance. However, this was done with data that was collected in a relatively short amount of time and with the human understanding that the thermal straining is the main reason for data fluctuation. To teach machine learning the complex loading, more field experiments are needed.

4. CONCLUSIONS & FUTURE STUDIES

This pilot study on developing wireless crack sensing system for bridges has successfully delivered the targeted sensing system with all functions including sensing, data processing, transmission, data interpretation, and abnormality detection. This system was achieved by integrating materials science (specifically nanomaterials), electrical engineering (specifically hardware on data acquisition and computer communication, power management), as well as computer science (specifically machine learning). The success of this project showed that current engineering solutions need a highly inter-disciplinary and convergence research, which does not only require the seamless integration of available engineering tools, but also novel development in all fields. Specifically, we developed new material synthesis approaches, new sensor fabrication process, new data acquisition approaches, as well as new data interpretation methods. With all these developments, we have showcased the practical application of a wireless crack sensing system for the department of transportation.

However, a few issues remain to be addressed. Due to the impact of COVID-19, the field implementation was compromised, which could reveal practice problems when installing and operating the developed system to the bridge sites. The potential issues include the durability of the bond between the sensor and the cracking surface, the reliability of the data transmission in rural areas with unstable cellular networks, and the battery maintenance for long term monitoring. These issues will be better solved in the future field experiments.

This research has produced 2 journal publications, which are in preparation, and 2 poster presentations in international conferences. The funding support from this project supported 1 Ph.D. student and 1 master student. The prototype sensors and data systems are ready to be transferred to the Missouri Department of Transportation through seminars and formatted documents and drawings.

5. REFERENCES

1.   NACE, *Corrosion Costs and Preventive Strategies in the United States*. National Technical Information Service, 5285 Port Royal Road, Springfield, VA 22161.

2.   Editorial. *HBM Strain Gauges: The First Choice for Your Strain Measurement*. [cited 2021; Available from: https://www.hbm.com/en/0014/strain-gauges/.

3.   Editorial. *Strain Gauge - Part 1*. 2009 2021]; Available from: https://engineers4world.blogspot.com/2009/10/stain-gague-part-1.html.

4.   Yin, Zhaozheng, Chenglin Wu, and Genda Chen, *Concrete crack detection through full-field displacement and curvature measurements by visual mark tracking: A proof-of-concept study.* Structural Health Monitoring, 2014. **13**(2): p. 205-218.

5.   Kharroub, Sari, Simon Laflamme, Chunhui Song, Daji Qiao, Brent Phares, and Jian Li, *Smart sensing skin for detection and localization of fatigue cracks.* Smart Materials and Structures, 2015. **24**(6): p. 065004.

6.   Huang, Haizhou, Shi Su, Nan Wu, Hao Wan, Shu Wan, Hengchang Bi, and Litao Sun, *Graphene-based sensors for human health monitoring.* Frontiers in chemistry, 2019. **7**: p. 399.

7.   Puértolas, JA, JF García-García, F Javier Pascual, José Miguel González-Domínguez, MT Martínez, and Alejandro Ansón-Casaos, *Dielectric behavior and electrical conductivity of PVDF filled with functionalized single-walled carbon nanotubes.* Composites Science and Technology, 2017. **152**: p. 263-274.

8.   Maity, Nirmal, Amit Mandal, and Arun K Nandi, *Interface engineering of ionic liquid integrated graphene in poly (vinylidene fluoride) matrix yielding magnificent improvement in mechanical, electrical and dielectric properties.* Polymer, 2015. **65**: p. 154-167.

9.   Editorial. *Teach, Learn, and Make with Raspberry Pi*. [cited 2021; Available from: https://www.raspberrypi.org/.

10.   Li, Yanxiao, Shuohan Huang, Congjie Wei, Chenglin Wu, and Vadym N Mochalin, *Adhesion of two-dimensional titanium carbides (MXenes) and graphene to silicon.* Nature communications, 2019. **10**(1): p. 3014.

11.   Chen, Shikun, Yanxiao Li, Dongming Yan, Chenglin Wu, and Nicholas Leventis, *Piezoresistive geopolymer enabled by crack-surface coating.* Materials Letters, 2019. **255**: p. 126582.

12.   Editorial. *Firebase Realtime Database*. 2021 [cited 2021; Available from: https://firebase.google.com/docs/database.

13.   Guo, Chuanrui, Yanxiao Li, Yanping Zhu, Chenglin Wu, and Genda Chen, *Synthesis and Characterization of Free-Stand Graphene/Silver Nanowire/Graphene Nano Composite as Transparent Conductive Film with Enhanced Stiffness.* Applied Sciences, 2020. **10**(14): p. 4802.

APPENDIX

This appendix contains additional figures for the sensor fabrication as well as the Python and MATLAB code for machine learning processing.
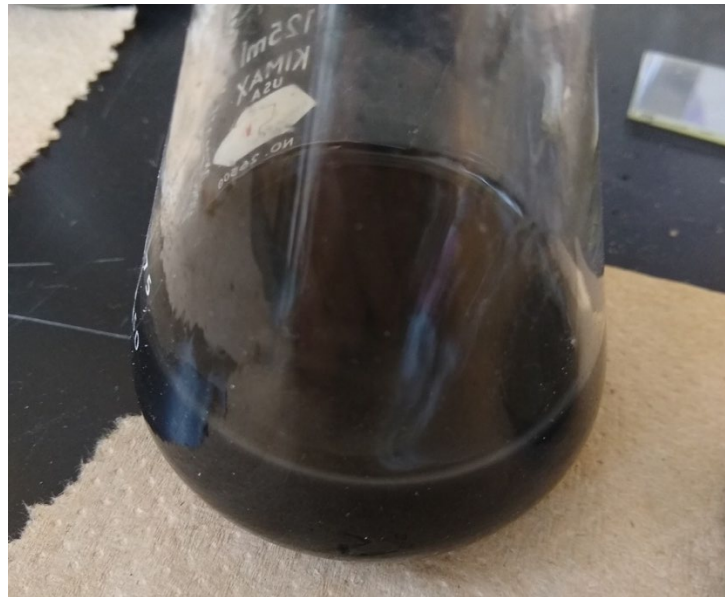

Fig. 25: Airbrush used to apply coating

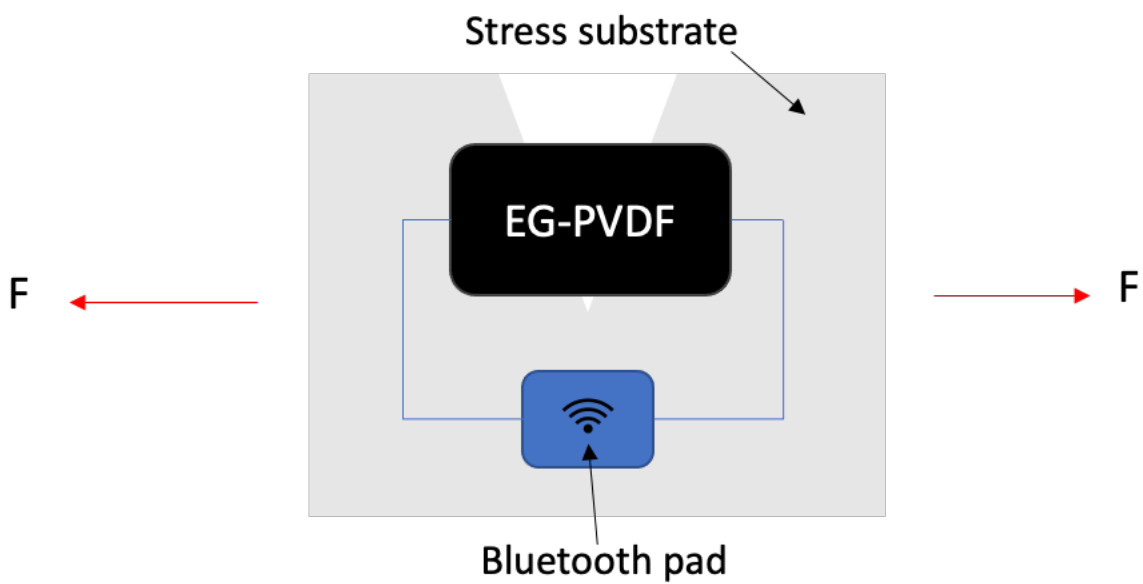**Fig. 26:** 8% PVDF/graphene suspension

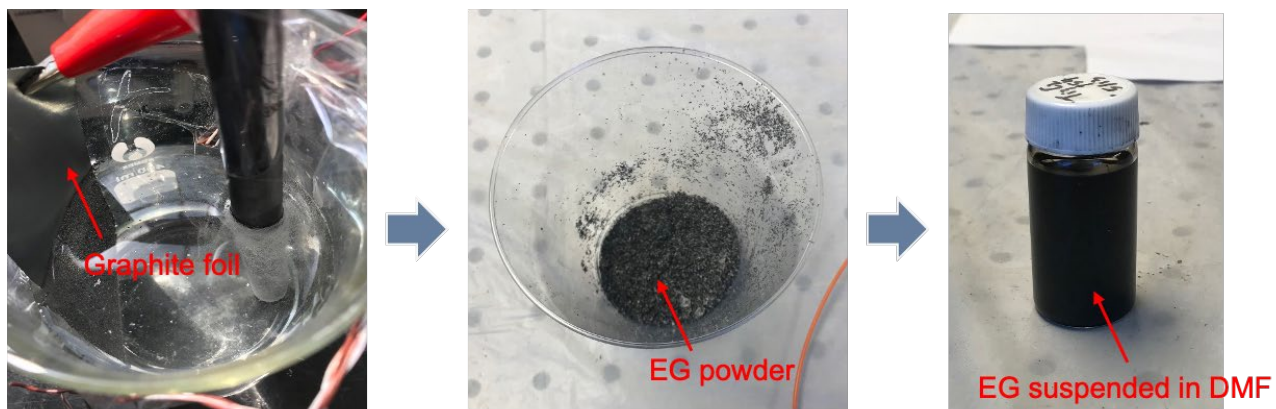**Fig. 27:** Alternative flexible sensing system design (unexplored)

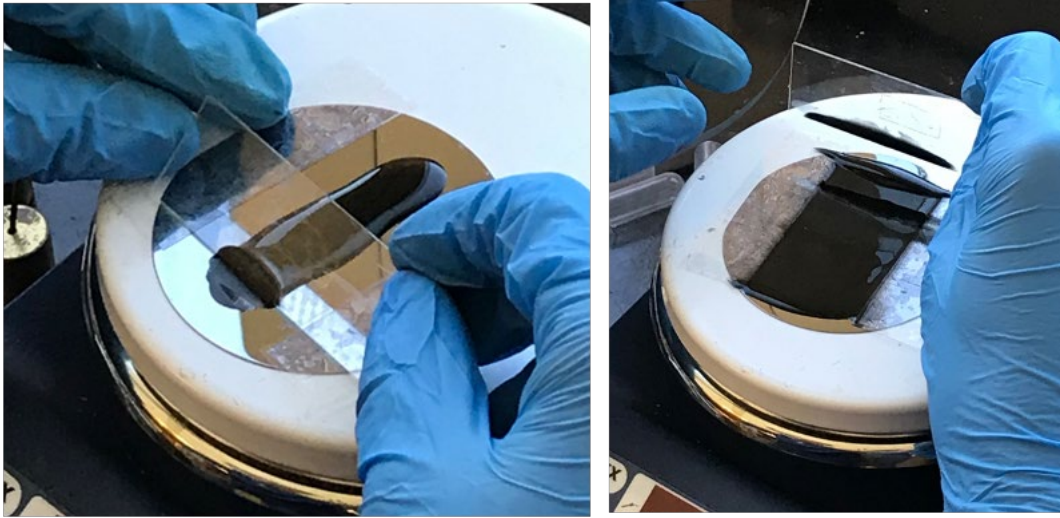**Fig. 28:** Electrochemical exfoliation of graphene process

Fig. 29: Preparing PVDF/graphene paste

Top view drop casting EG-PVDF Samples
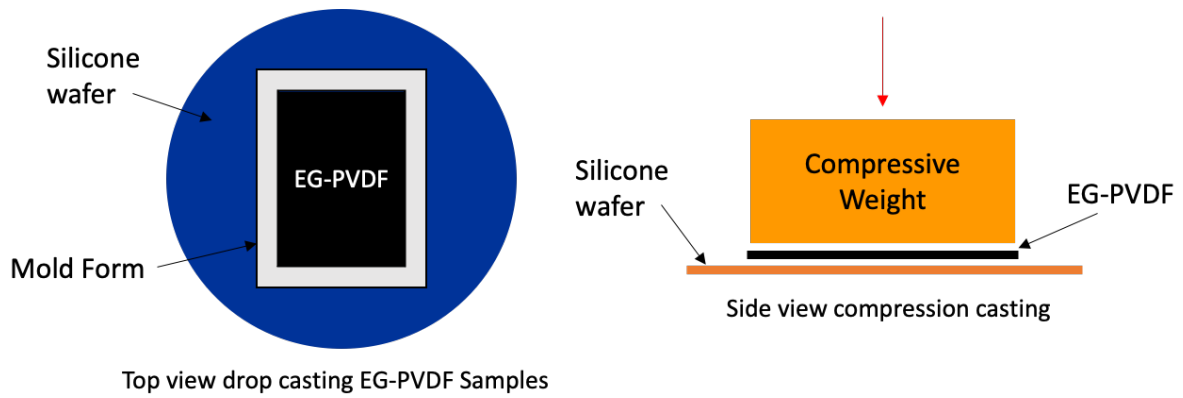
Side view compression casting

Fig. 30: Preparing PVDF/graphene paste: weighted curing

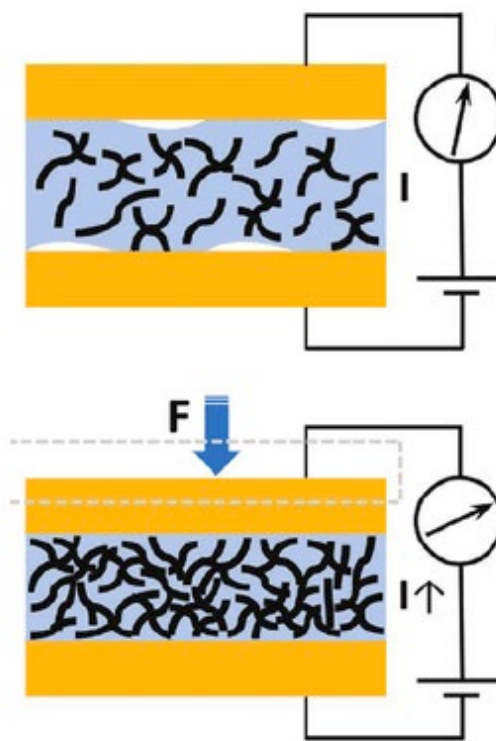**Fig. 31:** Dimension and structure of the thin film sensor

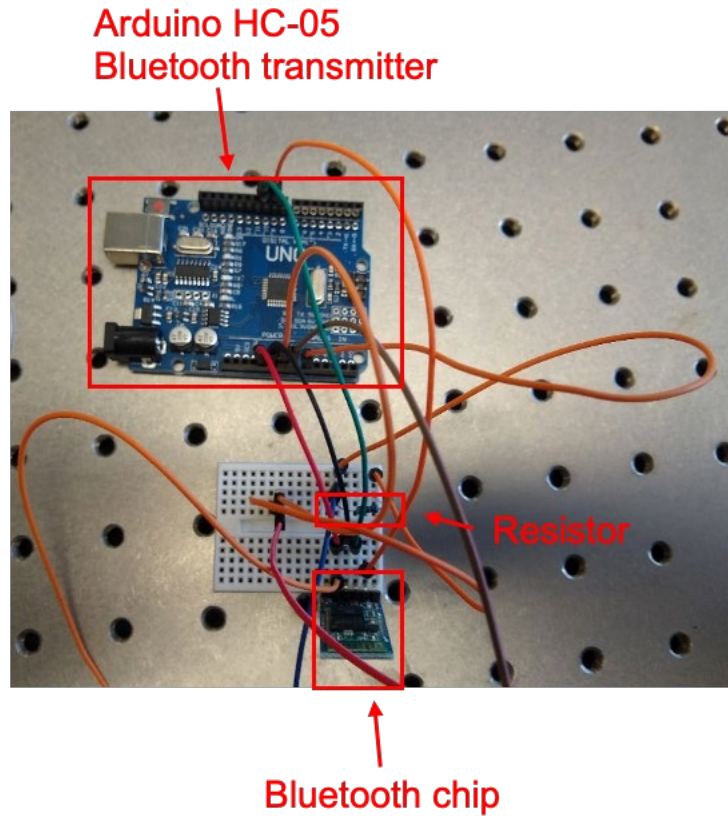**Fig. 32:** Piezoresistive sensing mechanism: dark lines are graphene
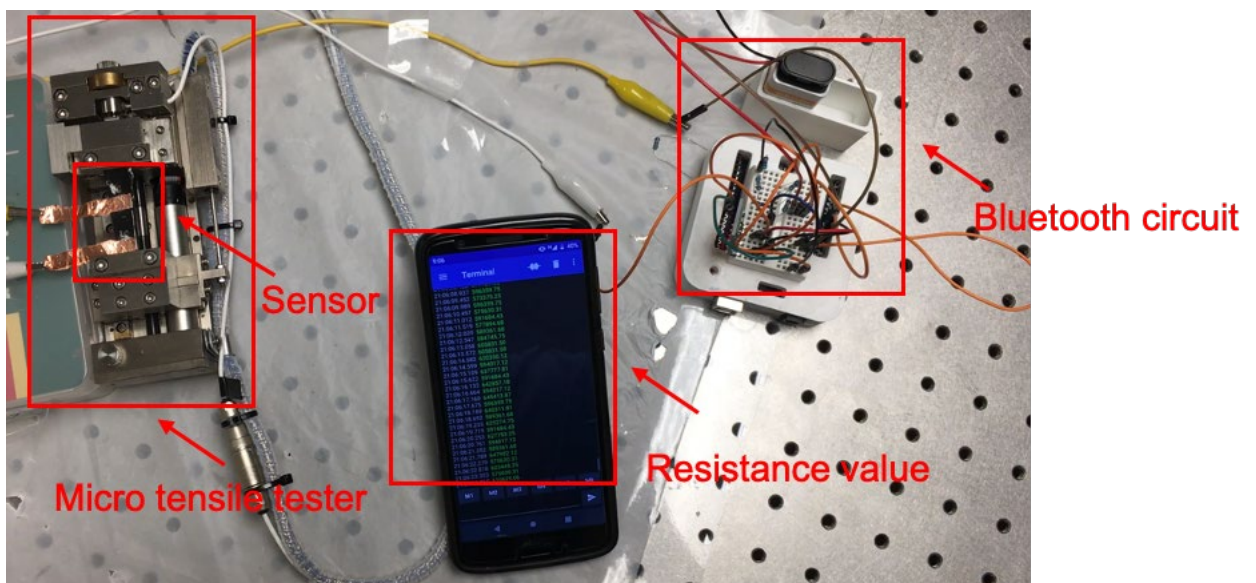
Fig. 33: Preliminary breadboard setup for DAQ

Fig. 34: Cellphone reading calibration using Bluetooth

Python Code

```python
# import

import numpy as np

import pandas as pd

import matplotlib

import matplotlib.pyplot as plt

from sklearn.neural_network import MLPRegressor

from sklearn.linear_model import Ridge

from mpl_toolkits.mplot3d import Axes3D

dataset=pd.read_csv('C:/users/westo/Desktop/sn1.csv')

X = dataset.drop('sn1', 1)

Y = dataset['sn1']

X1 = X['temp']

#X2 = X['delta']

# NN training function


def model_sales_MLP(dataset, hidden, print_coefs = True, max_iter= 10000000):

    num_samples = dataset.shape[0]

    cutoff = (num_samples * 26) // 27

    Xtrn = dataset.drop('sn1', 1).iloc[:cutoff,:]

    Ytrn = dataset['sn1'].iloc[:cutoff]

    Xval = dataset.drop('sn1', 1).iloc[cutoff:,:]
```

```python
    Yval = dataset['sn1'].iloc[cutoff:]

    model = MLPRegressor(hidden, validation_fraction = 0, solver='adam', max_iter=
max_iter).fit(Xtrn, Ytrn)

    coefs = model.coefs_

    yhat = model.predict(X)

    yhatval = model.predict(Xval)

    loss = np.square(Yval - yhatval).mean()

    hiddens = coefs[0].T

    final_mlp = coefs[1].flatten()

    coefs = list(zip([dict(zip(X.columns, h)) for h in hiddens],

                [['output mult:', m] for m in  final_mlp.flatten()],

                [['intercept:', i] for i in  model.intercepts_[0]]))

    print('loss:', loss)

    return model, yhat, coefs, loss
# NN learning and exporting to csv file
model, yhat, coefs, loss = model_sales_MLP(dataset, [2])

model, yhat, coefs, loss = model_sales_MLP(dataset, [2], max_iter = 50000000,
print_coefs=False)

model, yhat, coefs, loss = model_sales_MLP(dataset, [2], max_iter = 50000000,
print_coefs=False)

dataprint = pd.DataFrame({

    'yhat': yhat

}).round(5)
```

```python
dataprint.to_csv('C:/users/westo/Desktop/sn_norm.csv')

dataset1=pd.read_csv('C:/users/westo/Desktop/sn1-dndt.csv')

pred = model.predict(dataset1)

predprint = pd.DataFrame({

    'pred': pred

}).round(5)

predprint.to_csv('C:/users/westo/Desktop/sn_psid_norm.csv')
```

MATLAB Code

```matlab
dataset = xlsread('sn1.xlsx', 'Sn1', 'A1:B27');

x = dataset(:,1)';

t = dataset(:,2)';


% Choose a Training Function

% For a list of all training functions type: help nntrain

% 'trainlm' is usually fastest.

% 'trainbr' takes longer but may be better for challenging problems.

% 'trainscg' uses less memory. Suitable in low memory situations.

trainFcn = 'trainlm';  % Levenberg-Marquardt backpropagation.


% Create a Fitting Network

hiddenLayerSize = 50;

net = fitnet(hiddenLayerSize,trainFcn);
```

```matlab
% Setup Division of Data for Training, Validation, Testing

net.divideParam.trainRatio = 70/100;

net.divideParam.valRatio = 15/100;

net.divideParam.testRatio = 15/100;

% Train the Network

[net,tr] = train(net,x,t);


% Test the Network

y = net(x);

e = gsubtract(t,y);

performance = perform(net,t,y)


% View the Network
% view(net)
% Plots
% Uncomment these lines to enable various plots.
%figure, plotperform(tr)
%figure, plottrainstate(tr)
%figure, ploterrhist(e)
%figure, plotregression(t,y)
%figure, plotfit(net,x,t)
```